Journal of Medicinal Chemistry

Brief Article

pubs.acs.org/jmc

Repurposing Suzuki Coupling Reagents as a Directed Fragment Library Targeting Serine Hydrolases and Related Enzymes

Marion Lanier,*[,†] Derek C. Cole,[†] Yelena Istratiy,[†] Michael G. Klein,[‡] Phillip A. Schwartz,[‡] Richard Tjhen,[‡] Andy Jennings,[‡] and Mark S. Hixon*[,§,∥]

[†]Medicinal Chemistry - Gastrointestinal Drug Discovery Unit, [‡]Structural Biology & Biophysics, [§]Modeling & Simulation—Global DMPK, Gastrointestinal Drug Discovery Unit, Takeda California, Inc., 10410 Science Center Drive, San Diego, California 92121, United States

Supporting Information

ABSTRACT: Serine hydrolases are susceptible to potent reversible inhibition by boronic acids. Large collections of chemically diverse boronic acid fragments are commercially available because of their utility in coupling chemistry. We repurposed the approximately 650 boronic acid reagents in our collection as a directed fragment library targeting serine hydrolases and related enzymes. Highly efficient hits (LE > 0.6) often result. The utility of the approach is illustrated with the results against autotaxin, a phospholipase implicated in cardiovascular disease.

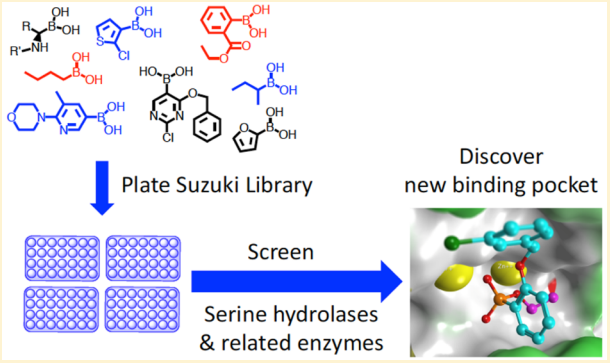

INTRODUCTION

Boronic acids are a staple of organic chemists thanks to the utility of Suzuki−Miyaura cross-coupling.[1−3] The widespread adoption of this coupling chemistry has led to the creation of large commercial boronic acid synthon libraries. These reagent libraries contain diverse alkyl or aryl boronic acids and esters substituted with various functional groups.

An intriguing feature of boronic acids is their ability to act as "serine traps" under the influence of a serine hydrolase's active site by forming metastable tetrahedral adducts with the catalytic serine.[4−6] Boron differs from carbon in that it has a vacant p-orbital that is receptive to dative bond formation with oxygen nucleophiles. Nucleophilic addition transforms boron from neutral trigonal planar to anionic tetraheadral.[7] The dative covalent complex is thought to resemble the catalytic mechanism's transition state on the path out of acyl−enzyme intermediate (Figure 1A). Mechanistically related enzymes such as autotaxin (ATX) are also inhibited by boronic acids although they have a catalytic threonine residue and stabilize the transient oxyanion through bimetallic oxyanion coordination (Figure 1B).

The common catalytic feature, i.e., transient covalent adduct formation with the side chain oxygen of serine or threonine, makes it likely that all serine hydrolases and mechanistically related enzymes are inhibited by small molecule boronic acids with appropriate complementarity.[8] It has been reported that the boronic acid motif will impart tight binding, frequently 100−1,000-fold greater if present than in its absence.[9]

The contribution of a boronic acid to a compound's potency when directed against a serine hydrolase is striking but alone, not sufficient to produce potent inhibition. Rather, the selectivity and potency of a boronic acid inhibitor arises from shape and interaction complementarities to the active site of the target.[10]

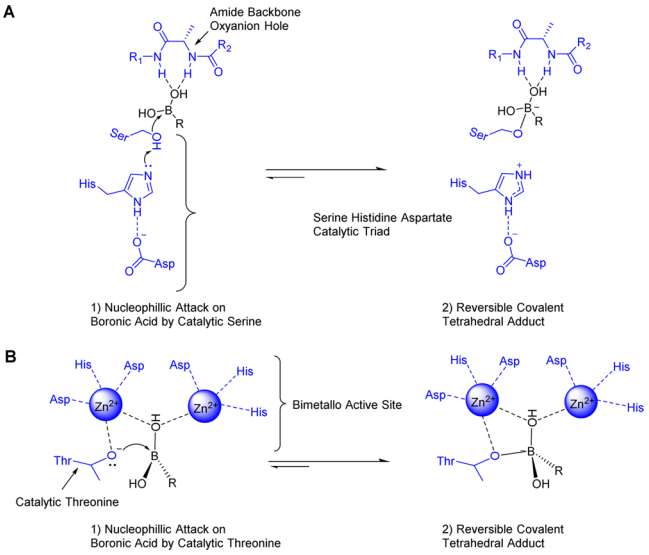

Figure 1. Boronic acid adduct formation with (A) a serine hydrolase; (B) ATX.

Received: September 26, 2016
Published: May 31, 2017

DOI: 10.1021/acs.jmedchem.6b01224
J. Med. Chem. 2017, 60, 5209−5215

Although tempted by the potency enhancement boronic acids offer when targeting susceptible enzymes, the pharmaceutical industry has, for the most part, been reluctant to develop boronic acid-based drugs out of fears of general toxicity and bioavailability.[11−13]

In contrast to these concerns, in 2003, Millennium Pharmaceutical's (now Takeda) bortezamib became the first FDA approved boronic acid-based drug. Bortezamib, intravenously administered, targets the 26S subunit of the proteosome and is used to treat relapsed multiple myeloma. In 2014, Anacor's tavaborole, which targets leucyl-tRNA synthetase, was approved by the FDA as a topical antifungal. In November of 2015, the FDA approved Takeda's ixazomib, an orally dosed proteosome inhibitor for treatment of patients with relapsed and/or refractory multiple myeloma. As more boronic acid-based inhibitors move through clinical trials and onto the market, the approach gains additional adherents.

In the quest for new drugs, fragment-based screening (FBS) offers great potential to generate inhibitors with drug like properties. FBS has been successfully applied to a number of targets, leading to the identification and approval of vemurafenib (PLX4032), a Plexxikon (now part of Daiichi-Sankyo) drug, as well as a number of fragment-derived drugs in the clinic.[14] A fragment library typically contains a few hundred to a few thousand compounds following the "Rule of Three" (MW < 300, the number of hydrogen bond donors is ≤3, the number of hydrogen bond acceptors is ≤3, and clogP ≤ 3).[15] Because fragments have fewer binding interactions with their target proteins than more elaborated inhibitors do, fragments typically have weaker binding. On the other hand, fragments of interest for lead generation bind more efficiently. A useful metric to capture this concept is ligand efficiency (LE), a measure of an inhibitor's affinity relative to its size.[16] Lipophilic ligand efficiency (LLE) is another efficiency metric linking potency and lipophilicity. Lipophilicity is known to influence the drug-like properties of a molecule.[17] Fragment hits are then elaborated using structural information to produce high affinity inhibitors in a superior drug-like space.

Like most pharmaceutical research institutions, Takeda has a large collection of boronic acid synthons because of their utility as chemical building blocks. We repurposed more than 650 boronic acid reagents as a directed fragment library and screen this library against serine hydrolases and related enzyme targets. The library provides wide chemical diversity around a number of scaffolds. By engaging the target enzyme's catalytic machinery, we obtain a substantial boost in ligand efficiency (affinity increases typically 100-fold) versus what is observed with an undirected fragment library.

There are reports of strategically incorporating boronic acids early in drug discovery campaigns.[18,19] The reported approaches screen undirected libraries to discover fragments or more elaborated inhibitors and then "direct" them by incorporating a boronic acid post hoc. Our approach differs in that we begin the screen with the core functionality (boronic acid) providing the directed library with a pronounced potency shift. As well, the boronic acid library samples the immediate region surrounding the target's catalytic machinery initiating the binding optimization process at the site of greatest affinity.

Determining the location and orientation of fragment hits within the target's active site is a key challenge in understanding the SAR of FBS. It is not uncommon for related fragments to have very different orientations within a binding pocket, thus requiring crystallography or protein NMR to resolve puzzling SAR. An important feature of the boronic acid directed approach is the known (assumed) point of attachment within the target enzyme's active site. The fixed point of attachment greatly reduces the number of possible poses, allowing computational studies to be more predictive in analyzing fragment SAR.

To illustrate the directed fragment library approach, we screened our boronic acid library against autotaxin (ATX), a lyso-phospholipase D enzyme that hydrolyzes lyso-phosphatidyl choline (LPC) into lyso-phosphatidic acid (LPA) (Figure 2). ATX has a conserved bimetallo active site containing two

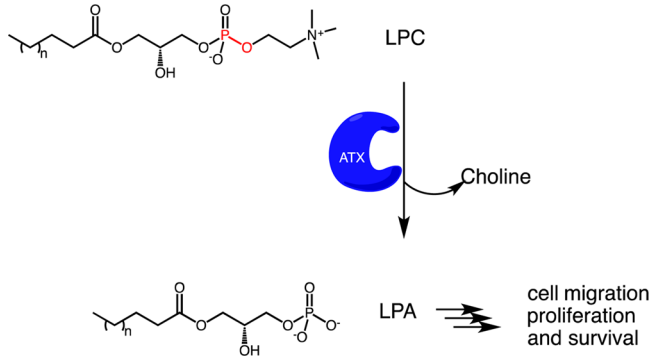

Figure 2. Autotaxin is responsible for the extracellular hydrolysis of LPC into the signaling LPA. LPA stimulates cell migration, proliferation and survival by binding to a distinct family of GPCRs (LPA1−-6), implicated in lymphocyte homing, chronic inflammation and fibrotic diseases.

Zn^{2+} ions (Figure 1B).[20,21] In ATX catalysis, threonine 209 is the nucleophile displacing choline in the first step of a double-displacement mechanism to produce an enzyme−phosphate intermediate. Next, the Thr209−LPA adduct is hydrolyzed by water to complete the catalytic cycle. In addition to aligning Thr209 and the phosphoryl group for in-line transfer, the two Zn^{2+} ions facilitate catalysis by activating the threonine and stabilizing charge buildup at the transition state (Figure 1B). Boronic acids with complementarity to the ATX active site are drawn into coordination with the bizinc complex and form a reversible covalent adduct with Thr209.

RESULTS AND DISCUSSION

The boronic acid library was screened at 100 μM in an ATX enzymatic activity assay. Hits (89), mostly selected for having a single point estimated pIC_{50} (−log of IC_{50} in molar units) ≥ 5 and LE ≥ 0.4, were then tested in an 11-point concentration response assay for confirmation. We identified and confirmed 51 hits possessing IC_{50}s ranging from 5 to 6.7. All confirmed hits with pIC_{50} > 4 contained an aromatic ring or a double bond attached directly to the boronic acid moiety.

Comparing the Boronic Acid Fragment Library (BAL) Hits to Biophysical Fragment Library (BPL) Hits. In addition to the BAL, we screened our fragment biophysical library[22] against autotaxin. The BPL is rule of 3 compliant and designed for biophysical screens such as surface plasmon resonance (SPR) and NMR. Screening was conducted at 500 μM with hits (143) then evaluated in an 11-point dose response assay.

Both fragment libraries have an average heavy atom count of 12. Upon calculating LE and LLE from the concentration response curve pIC_{50}s, the superior efficiency of the BAL

DOI: 10.1021/acs.jmedchem.6b01224
J. Med. Chem. 2017, 60, 5209−5215

compared to the BPL hits is evident (Figure 3). In FBDD, we strive to optimize LE and LLE. Plotting each hit's LLE versus its LE reveals the libraries form distinct clusters with the BAL clustering in a superior drug-like quadrant (Figure 3a). Examining LE, the BAL averages 0.2 greater ligand efficiency over the BPL (Figure 3b). Likewise, in the distribution about LLE, we find that the BAL centers a full log unit better than the BPL (Figure 3c). Given the hydrophobic nature of the ATX binding pocket, avoiding hydrophobicity in an inhibitor will be challenging, thus the contribution of boronic acid binding to the structure provides the advantage of an apparent one log unit offset in log *D*.

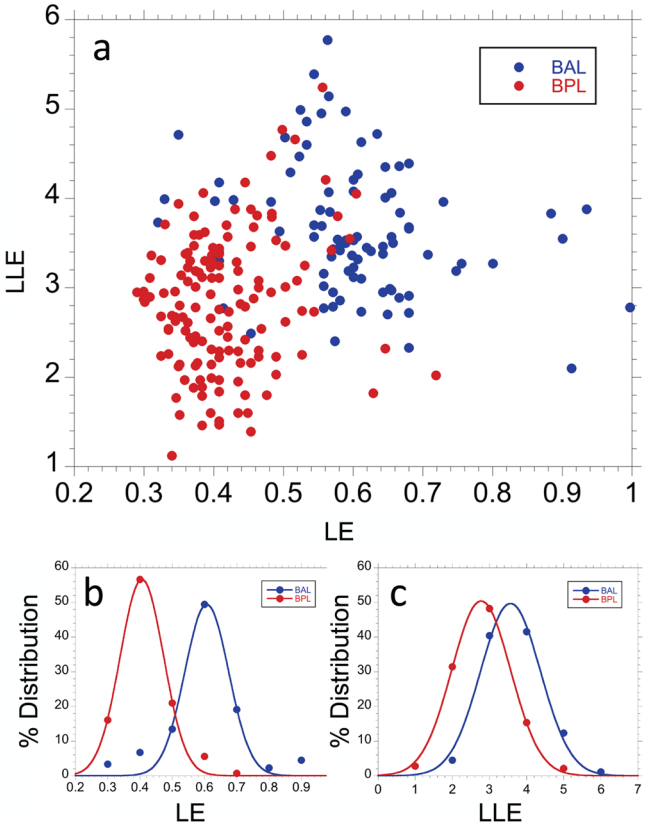

Figure 3. Hit distribution against ATX for our boronic acid (BAL) and biophysical libraries (BPL) as a function of ligand efficiency (LE) and lipophilic ligand efficiency (LLE) (a). The BPL has an average LE of 0.41, while the BAL LE averages 0.61 both libraries have a standard deviation of 0.1 (b). The LLE distribution of the libraries are distinct with the BPL library having an average LLE of 2.8 while the BAL library averages 3.6 both libraries have a standard deviation of 1.1 (c).

Hits from the libraries provide us with seven examples where the contribution of the boronic acid to binding can be compared with other functional groups including alcohol, carboxylate, and amine. As seen in Tables 1 and 2, on average, the boronic acid provides 100-fold greater affinity over that the same fragment containing a functional group other than boronic acid. This is not to imply the matched fragment pairs are binding in identical orientations. When targeting serine hydrolases and related enzymes, we frequently observe a shift in LE between the BAL and other fragment libraries. However, to date, we have not observed an enhanced potency shift between the BAL and other fragment libraries when they are screened against nonserine hydrolases (or mechanistically related targets). As well, occasionally the boronic acid fragments have failed to demonstrate enhanced potency versus other matched fragments such as carboxylate or hydroxyl when assayed against some serine hydrolases.

Table 1. Matched Fragment Pairs Comparing the Affinity of the Boronic Acid to Carboxylate or Alcohol

compound		pIC_{50}	compound		pIC_{50}
1	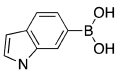	5.7 ± 0.02	3	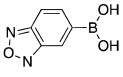	5.0 ± 0.02
2	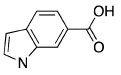	3.1 ± 0.04	4	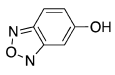	3.7 ± 0.03

Table 2. Matched Fragment Pairs around a Phenyl Core Illustrating the Potency Enhancement Provided by the Boronic Acid Functional Group

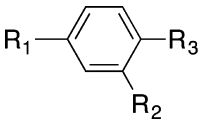

Compound	R_1	R_2	R_3	pIC_{50}
5		R-OH	H	5.0 ± 0.06
6		R-OH	H	2.9 ± 0.05
7		$R-NH_2$	H	4.9 ± 0.04
8		$R-NH_2$	H	3.6 ± 0.03
9		H	R-OH	5.0 ± 0.05
10		H	R-OH	3.3 ± 0.02
11		H		5.3 ± 0.04
12	R-OH	H		3.2 ± 0.07
13		H	$R-OCH_3$	5.3 ± 0.05

SAR Observations from the BAL Screen. The potencies and binding efficiencies of all compounds presented in this report are found in Table 3. The SAR observed around the phenyl core was largely consistent with a hydrophobic binding pocket, Figure 4, being representative of the hits. The core, phenyl boronic acid **14** has modest potency with a pIC_{50} of 5 but high binding efficiency with LE = 0.76 and a reasonable LLE of 3.4. Expanding ortho to the boronic acid, hydrophobic substituents were preferred as exemplified by **15** and **16**, with **16** increasing 10-fold in potency and maintaining LLE but with diminished LE. Similar SAR was observed in expansion from the meta position. In contrast to the overall affinity for hydrophobic substituents, hydroxyl **5**, amino **7**, and methylhydroxy **18** retained potency while methoxy **17** bound less avidly. Expanding further, **19** was 25-fold more potent than **18**. The SAR para to the boronic acid was comparable to that of meta as exemplified by **9**, **13**, and **22**.

DOI: 10.1021/acs.jmedchem.6b01224
J. Med. Chem. 2017, 60, 5209−5215

Table 3. Compound Potency (pIC_{50}), Ligand Efficiency (LE), and Lipophilic Ligand Efficiency (LLE)[a]

compd	pIC_{50}	LE	LLE
1	5.7	0.65	4.4
2	3.1	0.35	2.8
3	5.0	0.57	3.8
4	3.7	0.50	3.5
5	5.0	0.68	3.7
6	2.9	0.44	2.8
7	4.9	0.67	4.5
8	3.6	0.41	3.4
9	5.0	0.68	3.7
10	3.3	0.37	2.5
11	5.3	0.55	4.9
12	3.2	0.40	2.9
13	5.3	0.66	3.6
14	5.0	0.76	3.7
15	5.4	0.67	3.8
16	6.0	0.45	3.5
17	4.7	0.58	2.9
18	4.9	0.61	3.6
19	6.3	0.41	3.3
20	5.5	0.75	4.1
21	5.3	0.66	4.1
22	6.5	0.40	3.4
23	6.2	0.29	1.6
24	7.9	0.37	3.3
25	7.7	0.36	3.1
26	4.7	0.58	3.4
27	5.3	0.60	4.2
28	5.8	0.61	4.3

[a]Uncertainties in pIC_{50} are less than 0.1. Potencies for compounds **23**–**25** taken from Kawaguchi et al.[23].

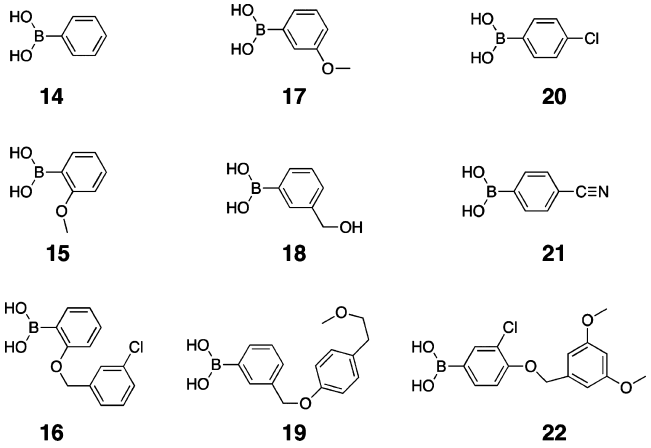

Figure 4. Representative SAR surrounding a phenylboronic acid core. See Table 3 for pIC_{50}, LE, and LLE.

The Nagano lab reported a series of ATX inhibitors including elaborations around a phenylboronic acid core.[23] Curiously, the same extended substituent when expanded meta or para to the boronic acid afforded comparable affinity with pIC_{50}s of 7.9 for **24** and 7.7 for **25**. On the other hand, when expanded ortho to the boronic acid as in **23**, affinity dropped 40-fold (Figure 5). The crystal structures of the bound complexes (PDBs 3WAX and 3WAY) provided in their report reveal differences in how the inhibitors occupy the active site of ATX. The ATX bound complexes with **22** and **23** form

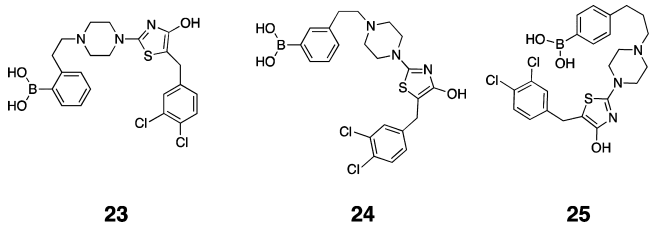

Figure 5. Reported bound ATX inhibitors with crystal structures from Kawaguchi et al.[23]

covalent adducts between the side chain oxygen of Thr209 and boron of the inhibitor. As well, one hydroxyl of the boronic acid coordinates with the catalytic zinc ions of the active site. The expanded tail, when directed meta or para, was accommodated within the hydrophobic channel of the active site. In contrast, the bound structure with **23** reveals an apparent steric clash with the walls of the channel, preventing simultaneous Thr209 adduct formation and occupancy of the hydrophobic channel. Thus, the bound complex of **23** occupies the channel without adduct formation and loses an apparent 40-fold potency versus **24** or **25**.

In contrast to the Nagano lab's SAR, BAL hits **16**, **19**, and **22**, representing expansions ortho, meta, and para to the boronic acid, have affinities within 3-fold of each other, with **16** possessing the highest LE of the three.

The binding interactions for some of our fragment hits were confirmed through crystallography of recombinant mouse ATX using published methods.[24] We obtained useful resolution (1.85 Å) for bound **16**. Binding of **19** was modeled based on a low resolution structure (3 Å; not described) and the crystallographic structures of **24** and **25**. The crystal structure of the ATX–**16** adduct revealed the boronic acid was coordinated to Thr209 and the catalytic zincs but, presumably due to steric clash, the benzoxy-ring was directed into an unreported pocket perpendicular to the hydrophobic channel (Figure 6).

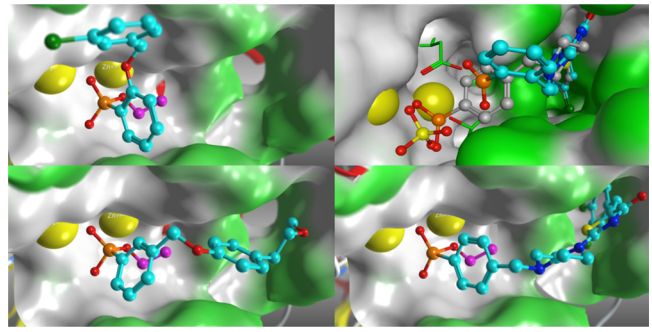

Figure 6. Crystal structures in mouse ATX. Crystal structure of **16** bound (top left) (PDB 5INH), crystal structure of **23** bound (top right), crystal structure of **19** bound (bottom left), and crystal structure of **25** bound (bottom right). Thr209 side chain is shown in purple, zinc ions are yellow, boron is tan, and surfaces are presented as green for hydrophobic and white for polar/charged.

Nitrile SAR. The nitrile series **26**–**28** produced some of the most promising SAR in the directed library screen. Moving from the nitrile to cyanomethylene increased potency 4-fold. Expanding further to the *E*-cyanovinyl **28** produced a fragment with a pIC_{50} of 5.8 (Figure 7). In this nitrile series, LE and LLE both improved in step with increasing potency.

DOI: 10.1021/acs.jmedchem.6b01224
J. Med. Chem. 2017, 60, 5209–5215

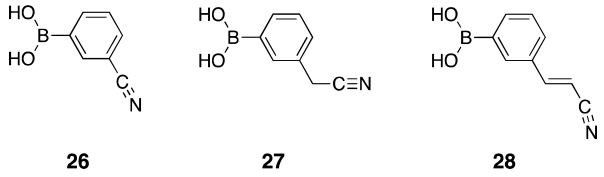

26 27 28

Figure 7. Selected nitrile series of phenyl boronic acids.

CONCLUSION

In summary, boronic acids form metastable tetrahedral adducts to the catalytic hydroxyl of serine hydrolases and related enzymes. Unrelated but fortuitously, Suzuki−Miyaura chemistry is widely used in the pharmaceutical industry and has given rise to the production of some 6000 commercially available chemically diverse fragment boronic acids. Like many other laboratories, we already possess a substantial collection of chemically diverse boronic acids and herein illustrate their repurposing as a directed fragment library containing substantial chemical diversity. The assumed point of attachment (covalent serine/threonine−boron adduct) greatly facilitates the contribution of computational chemistry to guide SAR in the absence of (or ahead of) crystallography. In this study, we have identified fragment leads recapitulating known SAR against ATX as well as discovering a previously unrecognized pocket (7). In addition, the nitrile series offer vectors for increasing potency while retaining ligand efficiency and lipophilic ligand efficiency.

EXPERIMENTAL SECTION

Compounds Procurement. Compounds **1**−**22** and **26**−**28** are commercially available from various venders and were used as is. Their structural integrities were determined by proton NMR. The purity of **1**−**6**, **8**−**12**, **18**, and **26**−**28** were assessed using HPLC. The purity of **7** was assessed using SFC. The purity of **13**−**17** and **19**−**22** were assessed using quantitative NMR. All compounds examined possess a purity of at least 95%. Details are available in Supporting Information.

Enzyme Activity Assays. ATX (full length human β form with a C-terminal 6-His tag) was purchased from Echelon Biosciences (Salt Lake City, UT; P/N E-4000). The BODIPY-FL labeled lysoPLD/autotaxin substrate FS-3 from Echelon Biosciences was used as substrate (Salt Lake City, UT; P/N E-4000). The ATX activity assay is based on the work of Ferguson el al.[25] All the concentrations of reagents described in the Experimental Section are final in the reaction media. Inhibition of ATX was measured in 20 mM Bis-Tris propane buffer at pH 8.0 containing 1 mM $MgCl_2$, 1 mM $CaCl_2$, 140 mM NaCl, 5 mM KCl, and 0.1% Triton X-405 (reaction buffer). Assays were performed at room temperature (~22 °C) with 1.6 nM ATX and 0.97 μM FS-3 substrate by monitoring the generation fluorescence after cleavage of the fluorogenic substrate. Inhibition was measured as a function of varying inhibitor concentration. Two assays were performed to assess inhibition of ATX, a single concentration point assay for screening compound libraries, and 11-point concentration response curves were generated in a continuous assay for detailed analysis.

In the end-point assay, 0.1 μL of library compounds were plated in Greiner low volume flat-bottom black 384-well plates. ATX was prepared in reaction buffer at twice the assay concentration, and 5 μL was dispensed via multidrop into the plate and incubated for 20 min. The assay was started by the addition of 5 μL of stock FS-3 solution, prepared at twice the assay concentration in reaction buffer. After 20 min, the assay was stopped by the addition of 5 μL of 150 mM EDTA in reaction buffer.

An 11-point concentration response curve was generated in a similar assay. ATX was prepared in reaction buffer at twice the assay concentration, and 50 μL was dispensed into black, flat bottom 96-well plates from NUNC. Then 1 μL of compound (varying concentrations) in DMSO was dispensed into the reaction mixture, mixed thoroughly by pipet, and incubated for 20 min. The assay was started by the addition of 50 μL of stock FS-3 solution, prepared at twice the assay concentration in reaction buffer. Measurement was initiated immediately in continuous mode.

The fluorescent assay was performed on a PHERAstar FE (BMG Labtech) microplate reader augmented with an FL 485 520 module for excitation at 485 nm while measuring emission at 520 nm in top optic mode. Gain was set to 545 and focal height was kept at 5.4 mm when using the 96-well NUNC plates and 10.8 mm when using the 384 Greiner plates. The pIC_{50} value is the geometric mean of at least two experiments unless otherwise stated.

Protein Expression and Purification. Murine ATX (residues 36−859) was cloned into the plasmid pFastBac1 engineered with an N-terminal signal sequence designed to target the recombinant protein for secretion and a C-terminal 6XHis linked by a TeV recognition sequence. The construct used for crystallization contained a deletion of residues 572−575 and two point mutations (I381E, T538E). Recombinant virus was generated using the Bac-to-Bac baculovirus expression system (Invitrogen). Media containing secreted mATX was concentrated and buffer-exchanged using diafiltration (Sartorius) into buffer composed of 20 mM Tris pH 8.0, 300 mM NaCl, and 0.2 mM $ZnCl_2$. Final concentrate was centrifuged for 20 min at 15000*g*, and the supernatant was affinity purified using Ni-chelating chromatography (ProBond, Life Technologies). The C-terminal 6XHis-tag was removed by treatment with TeV protease during an overnight incubation at 4 °C followed by size exclusion chromatography using a Superdex 200 column (GE Healthcare). Peak fractions from size exclusion chromatography were further purified using reverse-Ni chromatography. Purified fractions were pooled and buffer exchanged into buffer composed of 5 mM Tris pH 8.0 and 150 mM NaCl. Protein solution was concentrated with Amicon centrifugal filters (EMD Millipore) to 10 mg/mL and frozen in liquid nitrogen for storage at −70 °C.

Crystallography. Crystallization was performed using the hanging drop vapor diffusion method with a reservoir solution composed of 0.1 M sodium acetate (pH 4.5−5.5), 0.9 M $LiCl_2$, 0.2 M $ZnCl_2$, and 23−25% PEG 3350. Crystals were grown at 24 °C and reached maximum size after 2 weeks. Compound was soaked into apo-ATX crystals by adding 1 mM of compound in reservoir solution during an overnight incubation. Crystals were cryoprotected with reservoir solution containing 30% glycerol and flash-cooled in liquid nitrogen. Diffraction data were collected at Advanced Light Source beamline 5.0.3 (Lawrence Berkley's National Laboratory, Berkley CA) and processed with HKL2000.[26] The structure was solved by molecular replacement with Phaser[27] using the coordinates of mATX (PDB 3NKM) as a search model. The graphics program COOT[28] was used for model building, while refinement was performed with REFMAC5.[29] Phaser and REFMAC5 are distributed as part of CCP4.[30] Structure validation using Procheck revealed the residues fall in the most favored and allowed regions of the Ramachandran plot (89% and 11%, respectively) with no residues in the disallowed regions.

ASSOCIATED CONTENT

Supporting Information

The Supporting Information is available free of charge on the ACS Publications website at DOI: 10.1021/acs.jmedchem.6b01224.

Purity and characterization of all the compounds used (PDF)

Atomic coordinates are for ATX compound **19** model (PDB)

Molecular formula strings (CSV)

DOI: 10.1021/acs.jmedchem.6b01224
J. Med. Chem. 2017, 60, 5209−5215

AUTHOR INFORMATION

Corresponding Authors

*For M.S.H.: phone, 1 858 414-8750; E-mail, msh@mark-s-hixon-consulting.com.

*For M.L.: phone, 1 858 731-3552; E-mail, marion.lanier@takeda.com.

ORCID

Mark S. Hixon: 0000-0002-3525-0654

Present Address

‖For M.S.H.: Mark S. Hixon Consulting LLC, 11273 Spitfire Road, San Diego California 92126, United States.

Notes

The authors declare no competing financial interest.

ACKNOWLEDGMENTS

We thank Bi-Ching Sang for the construct encoding mATX; Eric Co, Jennifer Tsang, and Dan Scheibe for assembling the boronic acid library, Greg Warren of OpenEye for MOE (Chemical Computing Group; https://www.chemcomp.com renderings of several of the collected crystal structures. We also thank Gyorgy Snell and Wes Lane for collecting and processing the diffraction data; We thank the staff of the Berkeley Center for Structural Biology (BCSB) who operate ALS beamline 5.0.3. The BCSB is supported in part by the US National Institutes of Health, US National Institute of General Medical Sciences. The Advanced Light Source is supported by the Director, Office of Sciences, Office of Basic Energy Sciences of the U.S. Department of Energy under contract no. DE-AC02-05CH11231. Finally, we thank Stanley Yu for conducting the qHNMRs analysis or the compounds presented.

ABBREVIATIONS USED

ATX, autotoxin; bis-tris propane, 1,3-bis(tris(hydroxymethyl)-methyl)methylamino)propane; BODIPY-FL, 4,4-difluoro-4-bora-3a,4a-diaza-*s*-indacene fluorescence label; DMSO, dimethyl sulfoxide; clogP, computed log of the octanol–water partition coefficient; cpds, compounds; E, aspartic acid; EDTA, ethylenediaminetetraacetic acid; FBS, fragment-based screening; FDA, Food and Drug Administration; GPCR, G-protein coupled receptor; His, histadine; I, isoleucine; IC_{50}, inhibitor concentration producing 50% inhibition of vehicle control activity; LE, ligand efficiency; LLE, lipophilic ligand efficiency; LPA, lyso-phosphatidic acid; LPC, lyso-phosphatidyl choline; mATX, murine autotoxin; μL, 10^{-6} liter; mM, 10^{-3} molar; MW, molecular weight; nm, 10^{-9} meter; NMR, nuclear magnetic resonance; PEG, polyethylene glycol; PDB, Protein Data Bank; pIC_{50}, negative log of the IC_{50} expressed in molarity; SAR, structure–activity relationship; SFC, supercritical fluid chromatography; T, threonine; TeV, tobacco etch virus protease; Thr, threonine; Tris, tris(hydroxymethyl)-aminomethane

REFERENCES

(1) Suzuki, A. Carbon-carbon bonding made easy. *Chem. Commun.* **2005**, *38*, 4759–4763.

(2) Rouhi, A. M. Fine Chemicals Suzuki-coupling chemistry takes hold in commercial practice, from small scale synthesis of screening compounds to industrial production of active ingredients. *Chem. Eng. News* **2004**, *82*, 49–58.

(3) Maluenda, I.; Navarro, O. Recent developments in the Suzuki-Miyaura reaction. *Molecules* **2015**, *20*, 7528–7557.

(4) Philipp, M.; Bender, M. L. Inhibition of serine proteases by arylboronic acids. *Proc. Natl. Acad. Sci. U. S. A.* **1971**, *68*, 478–480.

(5) Bone, R.; Shenvi, A. B.; Kettner, C. A.; Agard, D. A. Serine protease mechanism: structure of an inhibitory complex of alpha-lytic protease and a tightly bound peptide boronic acid. *Biochemistry* **1987**, *26*, 7609–7614.

(6) Hunter, P. Not boring at all. Boron is the new carbon in the quest for novel drug candidates. *EMBO Rep.* **2009**, *10*, 125–128.

(7) Baker, S. J.; Tomsho, J. W.; Benkovic, S. Boron-containing inhibitors of synthetases. *Chem. Soc. Rev.* **2011**, *40*, 4279–4285.

(8) Smoum, R.; Rubinstein, A.; Dembitsky, V. M.; Srebnik, M. Boron containing compounds as protease inhibitors. *Chem. Rev.* **2012**, *112*, 4156–4220.

(9) Yin, Z.; Patel, S. J.; Wang, W. L.; Wang, G.; Chan, W. L.; Rao, K. R.; Alam, J.; Jeyaraj, D. A.; Ngew, X.; Patel, V.; Beer, D.; Lim, S. P.; Vasudevan, S. G.; Keller, T. H. Peptide inhibitors of Denegue virus NS3 protease. Part 1: Warhead. *Bioorg. Med. Chem. Lett.* **2006**, *16*, 36–39.

(10) Wienand, A.; Ehrhardt, C.; Metternich, R.; Tapparelli, C. Design, synthesis and biological evaluation of selective boron-containing thrombin inhibitors. *Bioorg. Med. Chem.* **1999**, *7*, 1295–1307.

(11) Trippier, P. C.; McGuigan, C. Boronic acids in medicinal chemistry: anticancer, antibacterial and antiviral applications. *MedChemComm* **2010**, *1*, 183–198.

(12) (a) Haas, M. J. Truly Boronic *SciBX* **2008**, *1*, doi: 110.1038/scibx.2008.840 and references therein. Assessing the oral bioavailablity of boronic acids is challenging because most reported compounds contain peptides or peptide-like moieties that are themselves poorly bioavailable. The boronic acid thrombin inhibitor DuP 714 orally dosed in dogs is 53% bioavailable. (b) Mitchell, T. J.; Knabb, R. M.; Christ, D. D.; Farmer, A. R.; Reilly, T. M. Analysis of the thrombin inhibitor DuP 714 by an enzyme-linked immunosorbent assay. *Blood Coagulation Fibrinolysis* **1994**, *5*, 517–521. Boronic acids are commonly prepared as esters of diols. In aqueous solution they rapidly hydrolyze to the boronic acid and conjugate diol (c) Kettner, C. A.; Shenvi, A. B. Inhibition of the serine proteases leukocyte elastase, pancreatic elastase, cathepsin G, and chymotrypsin by peptide boronic acids. *J. Biol. Chem.* **1984**, *24*, 15106–15114.

(13) Lesnikowski, Z. J. Recent developments with boron as a platform for novel drug design. *Expert Opin. Drug Discovery* **2016**, *11*, 569–578.

(14) Safety Study of PLX4032 in Patients With Solid Tumors. *ClinicalTrials.gov*; U.S. National Institutes of Health: Bethesda, MD, 2015; DOI: www.clinicaltrials.gov (accessed April 20, 2016).

(15) Congreve, M.; Carr, R.; Murray, C.; Jhoti, H. A 'rule of three' for fragment-based lead discovery? *Drug Discovery Today* **2003**, *8*, 876–877.

(16) LE = $-RT\mathrm{p}K_i$/nb heavy atoms. Hopkins, A. L.; Groom, C. R.; Alex, A. Ligand efficiency: a useful metric for lead selection. *Drug Discovery Today* **2004**, *9*, 430–431.

(17) LLE = pIC_{50} − cLogP. Leeson, P. D.; Springthorpe, B. The influence of drug-like concepts on decision making in medicinal chemistry. *Nat. Rev. Drug Discovery* **2007**, *6*, 881–890.

(18) Albers, H. M. H. G.; Dong, A.; van Meeteren, L. A.; Egan, D. A.; Sunkara, M.; van Tilburg, E. W.; Schuurman, K.; van Tellingen, O.; Morris, A. J.; Smyth, S. S.; Moolenaar, W. H.; Ovaa, H. Boronic acid-based inhibitor of autotaxin reveals rapid turnover of LPA in the circulation. *Proc. Natl. Acad. Sci. U. S. A.* **2010**, *107*, 7257–7262.

(19) Eidam, O.; Romagnoli, C.; Dalmasso, G.; Barelier, S.; Caselli, E.; Bonnet, R.; Shoichet, B. K.; Prati, F. Fragment-guided design of subnanomolar β-lactamase inhibitors active in vivo. *Proc. Natl. Acad. Sci. U. S. A.* **2012**, *109*, 17448–17453.

(20) Zalatan, J. G.; Fenn, T. D.; Herschlag, D. Comparative enzymology in the alkaline phosphates superfamily to determine the catalytic role of an active-site metal ion. *J. Mol. Biol.* **2008**, *384*, 1174–1189.

(21) Zalatan, J. G.; Fenn, T. D.; Brunger, A. T.; Herschlag, D. Structural and functional comparisons of nucleotide pyrophosphatase/

DOI: 10.1021/acs.jmedchem.6b01224
J. Med. Chem. 2017, 60, 5209–5215

phosphodiesterase and alkaline phosphatase: implications for mechanism and evolution. *Biochemistry* **2006**, *45*, 9788−9803.
(22) There are 1750 fragments with solubility >1 mM in phosphate buffered saline at 2% DMSO, pure by ^{1}H NMR, and nonreactive by SPR on a blank surface.
(23) Kawaguchi, M.; Okabe, T.; Okudaira, S.; Nishimasu, H.; Ishitani, R.; Kojima, H.; Nureki, O.; Aoki, J.; Nagano, T. Screening and X-ray crystal structure-based optimization of autotoxin (ENPP2) inhibitors, using a newly developed fluorescence probe. *ACS Chem. Biol.* **2013**, *8*, 1713−1721.
(24) Nishimasu, H.; Okudaira, S.; Hama, K.; Mihara, E.; Dohmae, N.; Inoue, A.; Ishitani, R.; Takagi, J.; Aoki, J.; Nureki, O. Crystal structure of autotoxin and insight into GPCR activation by lipid mediators. *Nat. Struct. Mol. Biol.* **2011**, *18*, 205−212.
(25) Ferguson, C. G.; Bigman, C. S.; Richardson, R. D.; van Meeteren, L. A.; Moolenaar, W. H.; Prestwich, G. D. Fluorogenic phospholipid substrate to detect lysophospholipase D/autotaxin activity. *Org. Lett.* **2006**, *8*, 2023−2026.
(26) Otwinowski, Z.; Minor, W. Processing of X-ray diffraction data collected in oscillation mode. *Methods Enzymol.* **1997**, *276*, 307−326.
(27) McCoy, A. J.; Grosse-Kunstleve, R. W.; Adams, P. D.; Winn, M. D.; Storoni, L. C.; Read, R. J. Phaser crystallographic software. *J. Appl. Crystallogr.* **2007**, *40*, 658−674.
(28) Emsley, P.; Cowtan, K. Coot: model-building tools for molecular graphics. *Acta Crystallogr., Sect. D: Biol. Crystallogr.* **2004**, *60*, 2126−2132.
(29) Murshudov, G. N.; Vagin, A. A.; Dodson, E. J. Refinement of macromolecular structures by the maximum-likelihood method. *Acta Crystallogr., Sect. D: Biol. Crystallogr.* **1997**, *53*, 240−255.
(30) Collaborative Computing Project. The CCP4 suite: programs for protein crystallography. *Acta Crystallogr., Sect. D: Biol. Crystallogr.* **1994**, *50*, 760−763.

DOI: 10.1021/acs.jmedchem.6b01224
J. Med. Chem. 2017, 60, 5209−5215